*Proc. Lunar Planet. Sci.*, 12B (1981), p. 1667–1687.
Printed in the United States of America

# Fragmentation of ice by low velocity impact

Manfred A. Lange and Thomas J. Ahrens

Seismological Laboratory, California Institute of Technology, Pasadena, California 91125

**Abstract**—Low velocity impact experiments (0.14 to 1 km/s) carried out in polycrystalline water ice targets at 257 and 81 K resulted in interactions which can be assigned to four fragmentation classes, cratering, erosion, disruption, and total fragmentation. Specific kinetic energies for the transitions between these classes range from $1\times10^5$ to $7\times10^5$ ergs/g for 81 K ice and from $3\times10^5$ to $\sim2\times10^6$ ergs/g for 257 K ice. These values are about one to two orders of magnitude below those for silicate rocks. The mass vs. cumulative number distribution of fragments in our experiments can be described by a simple power law, similar to that observed in fragmented rocks in both the laboratory and in nature. The logarithmic slopes of cumulative number vs. fragment weight vary between $-0.9$ and $-1.8$ decreasing with increasing projectile energy and are approximately independent of target temperature. The shapes of fragments resulting from erosion and disruption of ice targets are significantly less spherical for 257 K targets than for 81 K targets. Fragment sphericity increases with increasing projectile energy at 257 K, but no similar trend is observed for 81 K ice.

Our results support the hypothesis that the specific projectile energy is a measure for target comminution for a relatively wide range of projectile energies and target masses. We apply our results to the collisional interaction of icy planetary bodies and find that the complete destruction of a target body with radii between 50 m and 100 km range from $10^{17}$ to $10^{27}$ ergs. Energies corresponding to basaltic bodies of the same size range from $10^{18}$ to $10^{28}$ ergs. Our experiments suggest that regolith components on icy planets resemble those on rocky planetary bodies in size and shape. We predict that the initial shapes of icy particles in the Saturnian ring system were roughly spherical. The initial mass distribution of ring particles should follow a power law with a slope of $\sim -1.5$.

## 1. INTRODUCTION

An understanding of low velocity impact processes in targets of low temperature ice ($\sim$80 K) is important for both the accretion and surface evolution of icy planetary bodies, e.g., the Galilean and Saturnian satellites. Since impact velocities of accreting planetesimals are on the order of the escape velocity of an accreting body (Safronov, 1972), maximum impact velocities during accretion of the icy satellites did not exceed 0.15 to 2.7 km/s. The formation of a regolith layer is largely controlled by secondary impact cratering (Oberbeck, 1975). Secondary cratering on the smaller of the Saturnian satellites takes place primarily by the sweep-up of ejected debris from primary impacts. But here as in the case of the larger Galilean satellites, with escape velocities sufficient to retain primary ejecta, low velocity secondary impacts dominate the surface evolution on these bodies (Smith *et al.*, 1981).

In this paper, the following questions are addressed:

(i) What are threshold impact energies for transition between different stages of fragmentation of an icy body, as a function of temperature for decimeter sized targets?

(ii) What is the size distribution of particles resulting from impact fragmentation of an icy body as a function of temperature?

(iii) What are the shapes of these fragments, and do they change with varying target temperature?

The first problem is relevant to theoretical models describing the accretion of an icy planet and defines some of the physical parameters which define the conditions for mass accretion in contrast to mass loss during the growth of the planetary body. The latter two questions are relevant for the prediction of regolith characteristics on the surfaces of icy planets and, to a lesser degree, to the origin of icy planetary rings. The conclusions

inferred from the present experiments are, in principle, testable using radar and radio reflectance data of icy regoliths and ring particles (e.g., Pollack, 1975).

The fragmentation process of silicate bodies as well as that of water ice at temperatures close to the freezing point has been experimentally studied to some degree by Gault and Wedekind (1969), Fujiwara *et al.* (1977) and Hartmann (1978). In order to compare impact events in which the projectile to target mass ratio is varied, the specific kinetic energy, *ke*, of the projectile, i.e., its kinetic energy divided by the target mass has been defined (Gault and Wedekind, 1969; Fujiwara *et al.*, 1977). Projectile kinetic energy divided by target volume has the dimension of strength, i.e., supportable force/area and has been called impact strength (Greenberg *et al.*, 1978). Although this quantity is conceptually different from the strength of a material in the sense of a quasi-static test, it is helpful in visualizing the magnitude of a particular impact event. In this paper we use *ke* to denote projectile kinetic energy divided by target mass. Critical values for *ke* which lead to the destruction of an impacted glass, basalt, and ice target are given as $10^7$, $6 \times 10^7$, and $3 \times 10^5$ ergs/g, respectively (Gault and Wedekind, 1969; Fujiwara *et al.*, 1977; Hartmann, 1978). However, it is expected that the physical properties of $H_2O$ ice, controlling its behaviour under shock loading in the temperature range of interest in this study (i.e., at $\sim 80$ K), are different from the aforementioned materials. It should be noted here that the result for water ice, as given by Hartmann (1978) represents a different experimental approach than that of Gault and Wedekind (1969), Fujiwara *et al.* (1977) and the present study. Hartmann studied the destruction of ice by firing or dropping centimeter-scale ice projectiles onto flat rock targets with velocities in the range of 1 to 50 m/s. Hence, the critical energy for the destruction of ice represents kinetic projectile energy/*projectile* mass. But not only are Hartmann's experiments conceptually different, they also attempt to simulate the interaction of ice with silicate bodies, whereas we are studying primarily the interaction between icy bodies. Hence, the above given data on critical impact energies for glass, basalt, and ice will serve as a basis for comparison with our experimental results presented below.

Experimental data for the quasi-static deformation of polycrystalline ice indicate an increase in compressive strength from 20–25 bars to $\sim 80$ bars and an increase in tensile strength from 15 to 25 bars for temperatures between 273 and 223 K, respectively (Hobbs, 1974). However, these data are obtained at stress rates of $\sim 5$ bars/s (Butkovich, 1954), which are orders of magnitude below the rates of kilobars to tens of kilobars per second typical of low velocity impacts. Since it is known that the strength of ice is highly stress rate dependent (Hobbs, 1974), we will not use these data in the present study.

We performed low velocity impact experiments on polycrystalline water ice targets mainly at temperatures of 257 and 81 K. In the following, we briefly describe our experimental techniques and results. We discuss these results and how they may apply to impact and fragmentation processes of icy planetary bodies.

## 2. EXPERIMENTAL TECHNIQUES

The majority of our cubic target blocks ($\sim 19$ cm sidelength) had temperatures of either 257 or 81 K. Blocks of 257 K were prepared following the technique described by Croft *et al.* (1979) in order to eliminate air bubbles in the sample. The container was then placed in a freezer at temperatures of $\sim 257$ K and remained there for several days until immediately before the experiment. A major problem in the preparation of the 81 K targets was the formation of thermoelastic induced cracks as the sample was cooled. They are caused either by volume expansion of inner, solidifying parts or by the contraction of solid outer portions of the sample which had lower temperatures due to their proximity to the coolant. A water filled plastic container was placed directly in a liquid nitrogen bath of 77 K. Crystal growth started at the bottom and along the walls of the container, and continued inward and upward. In order to avoid extensive cracking of the sample blocks, we inhibited the growth of ice crystals on the upper liquid surface. As cooling progressed, the remaining fluid was continually stirred, until the entire water volume solidified. In most cases, the surface of the freezing block was kept fluid until the temperature in the ice reached $\sim 150$ K. At this point, most of the volume expansion of solidifying water had occurred. For the temperature range from 273 to 150 K, the volume of ice-I decreases by $\sim 1.5\%$, while the contraction for temperatures between 150 and 81 K amounts to $\sim 0.3\%$ (Hobbs, 1974). Hence most of the total volume

**Table 1.** Basic experimental data.

| Shot No. | Target Mass $M_T$, g | Target Temp. $T_T$, K | Impact Velocity $v_i$, km/s | Projectile specific kinetic energy *ke*, $10^5$ ergs/g | Peak impact stress $\sigma$, kbar* |
|---|---|---|---|---|---|
| 570 | 5900 | 81 | 1.05 | 56.83 | 24.03 |
| 571 | 5571 | 257 | 1.04 | 59.36 | 22.63 |
| 590 | 5458 | 257 | 0.24 | 4.40 | 5.57 |
| 591 | 5797 | 257 | 0.14 | 1.35 | 3.13 |
| 592 | 5930 | 81 | 0.23 | 3.70 | 5.91 |
| 593 | 6043 | 257 | 0.16 | 1.74 | 3.83 |
| 596 | 4657 | 81 | 0.27 | 6.20 | 6.65 |
| 597 | 6410 | 257 | 0.29 | 4.92 | 6.61 |
| 598 | 5754 | 257 | 0.35 | 7.13 | 8.01 |
| 602 | 6832 | 257 | 0.21 | 2.50 | 4.87 |
| 604 | 5882 | 81 | 0.18 | 2.24 | 4.44 |
| 605 | 6634 | 257 | 0.30 | 5.40 | 6.96 |
| 609 | 6024 | 257 | 0.51 | 17.70 | 11.49 |
| 611 | 5673 | 81 | 0.16 | 1.72 | 3.70 |

*Peak one-dimensional stresses are calculated based on Hugoniot data for ice-I by Anderson (1968) and on the elastic parameters of ice as a function of temperature given by Dantl (1969).

change could be relieved until the surface of the block closed up. The temperature in the ice was monitored by use of a thermocouple placed in the center of the target block.

The target blocks were placed inside a steel tank, under ambient pressure conditions, directly in front of the evacuated barrel of a conventional 20 mm powder gun. The blocks were impacted immediately after removal from the coolant (or from the freezer); during this interval, the increase in temperature of the blocks was insignificant (less than ~5 degrees). Cylindrical Lexan (a polycarbonate plastic, density = 1.2 g $cm^{-3}$) projectiles were used in these experiments. In order to cover a relatively wide range of specific kinetic energies, we varied the impact velocities of the projectiles from 0.14 to 1.05 km/s keeping both target and projectile mass nearly constant. Specific kinetic energies of the projectiles ranged from $1.4 \times 10^5$ to $\sim 60 \times 10^5$ ergs/g (Table 1). Immediately after the impact, the fragmented target block was photographed and a number of samples from different positions in the tank were taken for further analysis. The degree that secondary impact of fragments with the steel wall of the tank affected the fragment population is not known. In general, we tried to collect as many fragments with sizes ≥ cm as possible (with the exception of shots 570, 571, and 611 where a representative collection of fragments were taken). The remaining, smaller fragments were collectively weighed. The larger specimens were individually weighed and the short, intermediate, and long axes of each fragment (= C, B, and A, resp.) were measured by means of a slide caliper. The error in fragment masses is not greater than ± 1 g and the lengths are accurate within ± 1 cm.

## 3. RESULTS

The present experiments resulted in fragmented target blocks which can be assigned to four fragmentation classes defined below. These are comparable to the destruction types given by Fujiwara *et al.* (1977) for impact experiments on basaltic targets. However, fragmentation according to their destruction type II (i.e., spallation of outer surfaces with remaining core also called core type) was not observed in our experiments. We define the following fragmentation classes based on the ratio between mass of largest fragment $M_{lf}$ to original target mass ($M_T$):

### I. Total destruction

The entire target block has been comminuted into fragments not exceeding sizes of ~10 cm. The bulk of the fragments have mean sizes between 2.5 and 9 cm. In this class, the mass of the largest fragment is less than 0.03 times the target mass (i.e., $M_{lf}/M_T \leq$

1982LPSC...12.1667L



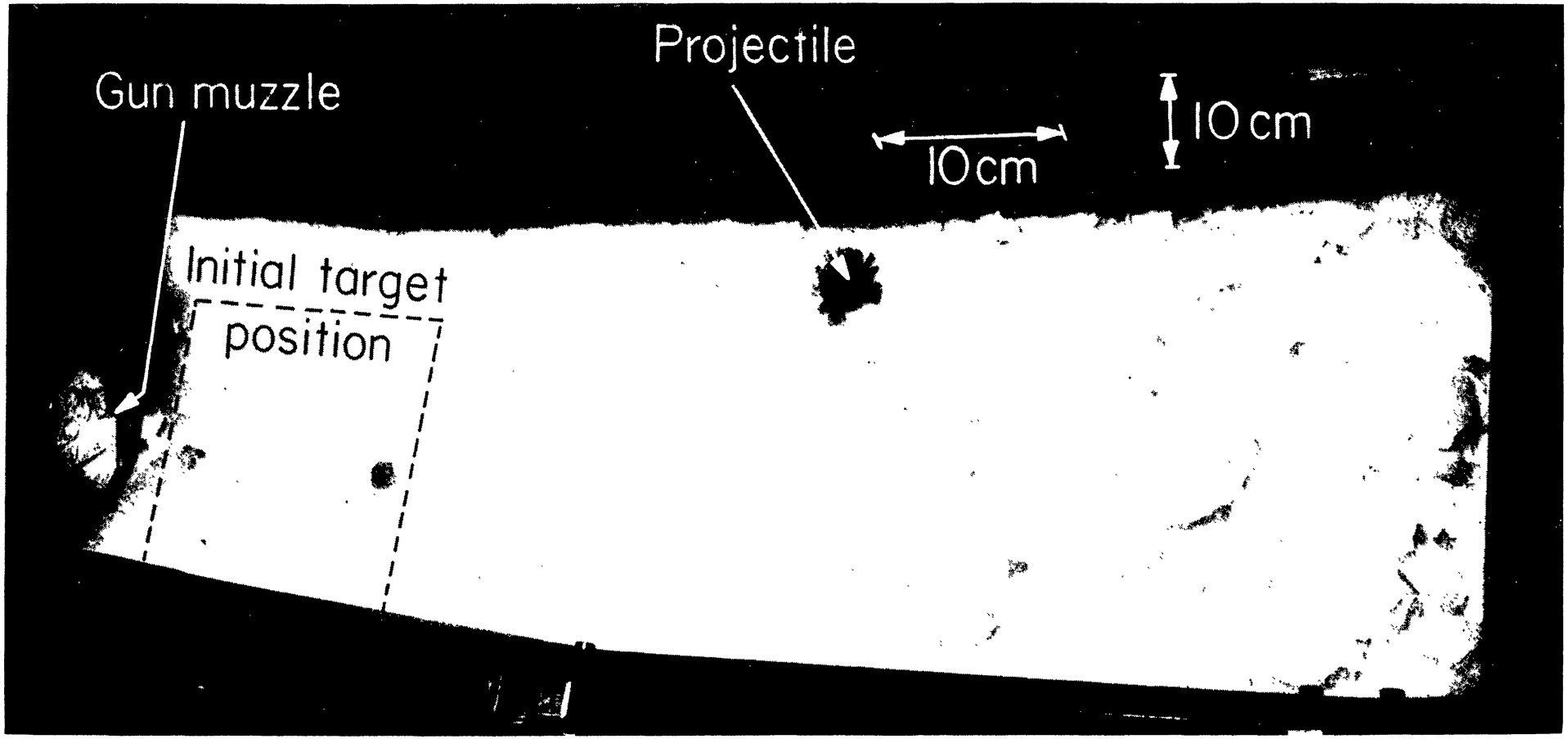


**Fig. 1.** Total fragmented ice target (Shot No. 570, 81 K). Initial target block was placed as shown. Impact achieved from Lexan projectile traveling from left to right. (See text and Table 1 for further details).

0.03). Figure 1 shows a typical example of class I fragmentation. The cumulative number of sampled fragments for class I experiments as a function of relative fragment mass is given in the left part of Fig. 5.

## II. Disruption

This type is characterized by the target block being split into generally two to three larger fragments and a great number of small fragments. The mass of the largest fragment in this class varies from 0.03 to 0.3 times the original target mass (i.e., $0.03 < M_{lf}/M_T \leq 0.3$). Figure 2 gives a representative example of class II fragmentation and the center part of Fig. 5 shows the results for all class II experiments.

## III. Erosion

This fragmentation type is intermediate between cratering and disruption of the target block. Generally, parts of the target, adjacent to the impact point, are spalled off, while most of the target block remains intact. Impacts in this class result in eroded blocks greater than 0.3 times the original target mass (i.e., $1 > M_{lf}/M_T > 0.3$). A typical example of this class is given in Fig. 3, the right part of Fig. 5 summarizes our results for class III fragmentation.

## IV. Cratering

Impacts in this class result in the formation of a crater of varying dimensions and leave the target block intact (see Fig. 4; i.e., $M_{lf}/M_T \sim 1$).

Although the boundaries between the four fragmentation classes, defined as a particular ratio between the mass of the largest fragment to original target mass, seem—at this point—somewhat arbitrary, the results of our experiments confirm the utility of these definitions.

Table 2 gives the results of our experiments. The recovered target fraction (column 3) includes the collectively weighed smaller samples, as well as the individually weighed fragments. D and h (columns 7 and 8) are the diameter and depth of the craters for the type IV experiments.

In the following, the distribution of fragment masses and fragment shapes for the experiments in classes I–III are discussed. Class IV experiments are described elsewhere (Lange and Ahrens, 1981).

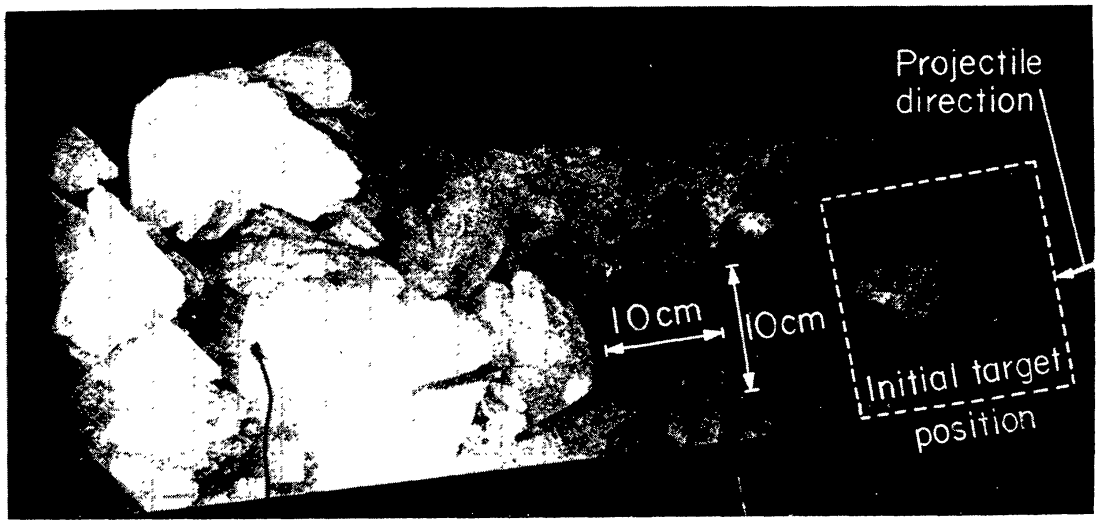


**Fig. 2.** Disrupted ice target (Shot No. 598, 257 K); configuration of initial target block as shown.

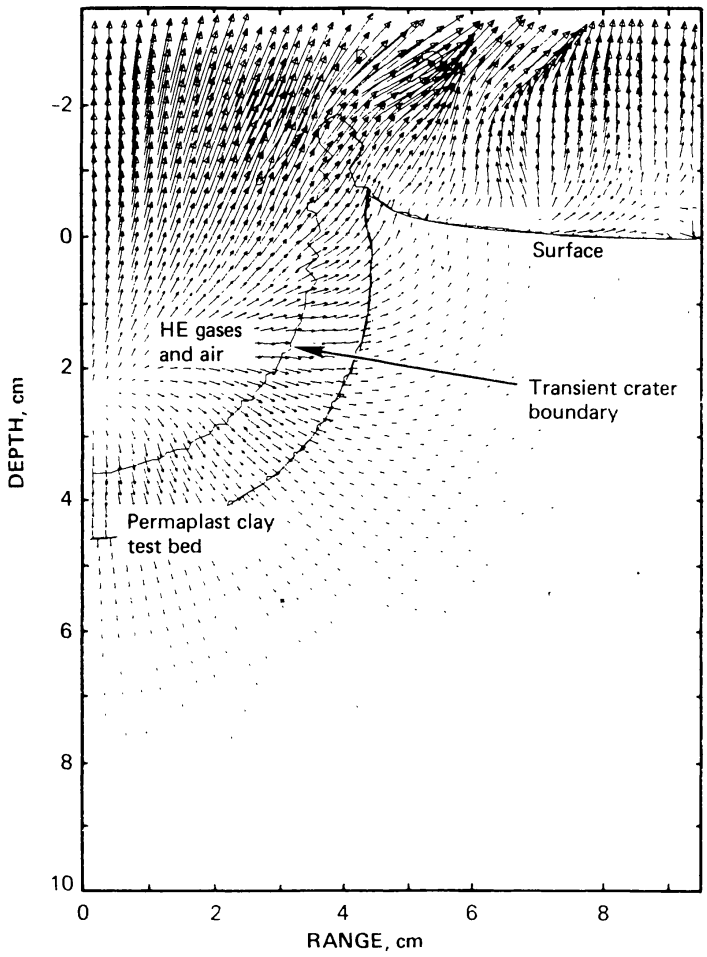


**Fig. 14.** Vector velocity and material boundary plot at 100 $\mu$sec for the 25-X calculation.

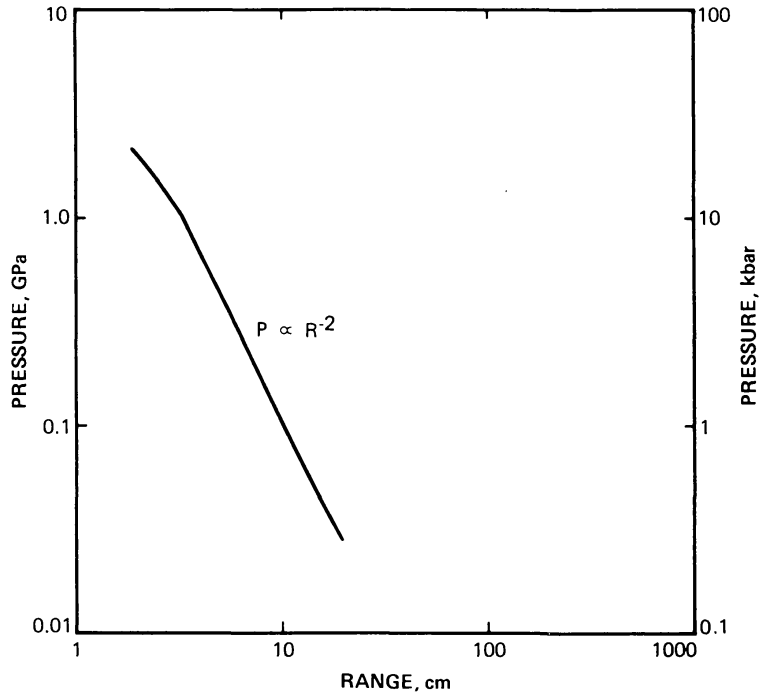


**Fig. 15.** Maximum shock pressure in target versus range in the downward direction from the 25-O and 25-X calculations.


**Fig. 4.** Crater formation in ice (Shot No. 602, 257 K). The impact point is clearly seen as a central pit inside the crater. The target block was sprayed with black paint to enhance contrast after impact.

of fracturing (i.e., decreasing number of fragmentation class), lying at $\sim 1.6$, $\sim 1.2$, and $\sim 0.9$ for class I, II, and III, respectively. The dependence of b on target temperature is less obvious. The mean values of b for class I and II experiments of 81 K targets are 12% and 19% higher than for the 257 K targets. b values for class III fragmentation are essentially independent of target temperature.

Hartmann (1969) has compiled data describing the fragmentation of terrestrial and extraterrestrial rocks by a variety of natural processes. b values for terrestrial rocks range from 0.6 to 1.2. Values for the ejecta of hypervelocity impacts vary between 1.0 and 1.2. b values for (presumably impact) debris on the lunar surface lie between 0.7 and 1.1. Hence, these rock fragments from different environments yield mass-number characteristics similar to the present class II and III fragmentation.

Fujiwara *et al.* (1977) report for impact experiments in basaltic targets b values between 1.05 and 1.4 for fragment sizes from 2 mm to 1 cm. These agree well with our b values for classes I to III.

**Table 2.** Major experimental results.

| Shot No. | *ke*, $10^5$ ergs | Fragm. Type | Recovered Target Fraction, % | Mass of Samples < 1 cm g | Mass of Samples > 1 cm, g | Mass of Single Fragment, g | D*, cm | h*, cm |
|---|---|---|---|---|---|---|---|---|
| 570 | 56.83 | I | 15 | — | 899 | — | — | — |
| 571 | 59.36 | I | 7 | — | 411 | — | — | — |
| 590 | 4.40 | III | 86 | — | 642 | 4050 | — | — |
| 591 | 1.35 | IV | — | — | — | — | 8.0 | 1.3 |
| 592 | 3.70 | II | 100 | 1790 | 1666 | 2472 | — | — |
| 593 | 1.74 | IV | — | — | — | — | 8.9 | 1.6 |
| 596 | 6.20 | II | 99 | 2153 | 2244 | — | — | — |
| 597 | 4.92 | III | 97 | 650 | 802 | 4789 | — | — |
| 598 | 7.13 | II | 100 | 1407 | 1243 | 3104 | — | — |
| 602 | 2.50 | IV | — | — | — | — | 10.8 | 1.3 |
| 604 | 2.24 | III | 98 | 1796 | 1201 | 2815 | — | — |
| 605 | 5.40 | III | 97 | 412 | 750 | 5265 | — | — |
| 609 | 17.70 | I | 96 | 4330 | 1477 | — | — | — |
| 611 | 1.72 | III | 99 | 1368 | 820 | 3415 | — | — |

*Diameter D and depth h of craters in class IV fragmentation.

The differences in impact fragmentation (for fragmentation types I to III) as a function of target temperature are shown in Fig. 8. As can be seen, the spread in fragment masses in the range from ~5 to ~100 g is significantly smaller for targets of 81 K than for 257 K targets. It can also be seen that the total number of fragments is generally smaller for the warmer targets. This does not represent incomplete sampling, as might be expected, but reflects the fact that fragments in the ~5 to ~30 g range are more numerous for targets initially at 81 K than for targets with a temperature of 257 K. Thus, while the relative distribution of fragment masses in each fragmentation class is nearly independent of temperature (i.e., the values for b do not vary greatly as a function of target temperature), the absolute number of fragments for each fragment mass is larger for an 81 K target, as compared to a 257 K target. This fact is reflected in the C values, which are larger for the 81 K targets than for the 257 K targets (see Table 3).

## 3.2 Fragment shapes

The ratios of intermediate to long axes (B/A) versus the ratio of short to long axes (C/A) for fragments from six experiments and mean values are shown in Fig. 9. Here B/A and C/A are called shape factors. The upper diagrams give the shape factors for targets with temperatures of 257 K, the lower ones are for 81 K targets. Roughly spheroidal or, equant, fragments will have $B/A = C/A = 1$, whereas platy fragments have $B/A \rightarrow 1$ and $C/A \rightarrow 0$, and elongated rods have $B/A \rightarrow 0$ and $C/A \rightarrow 0$. Mean values for B/A and C/A are given in Fig. 10 and Table 3. As can be seen, there is a clear distinction between the fragments of 257 K targets as compared to those of the colder targets. With the exception of class I fragmentation, the mean values of the shape factors are larger for the 81 K targets than for the 257 K targets. While the fragmentation type is of no significant influence on B/A vs. C/A for the 81 K targets, there is a transition from more bar-like fragments in class III fragmentation to more spherical fragments in class I experiments for the 257 K targets. The results for the targets with temperatures of 81 K are in agreement with the mean values of B/A and C/A obtained by Fujiwara *et al.* (1978) for basaltic targets. These values (coinciding with the point for our shot 604) represent the means for a total of 719 fragments greater than 4 mm from catastrophically destroyed targets with remaining cores (destruction type II of Fujiwara *et al.*, 1977). Hartmann and Cruikshank (1978) report values of B/A for 46 fragments produced in collisional fragmentation experiments on igneous rocks at velocities between 26 and 50 cm/s and find a mean value for $B/A = 0.71$.

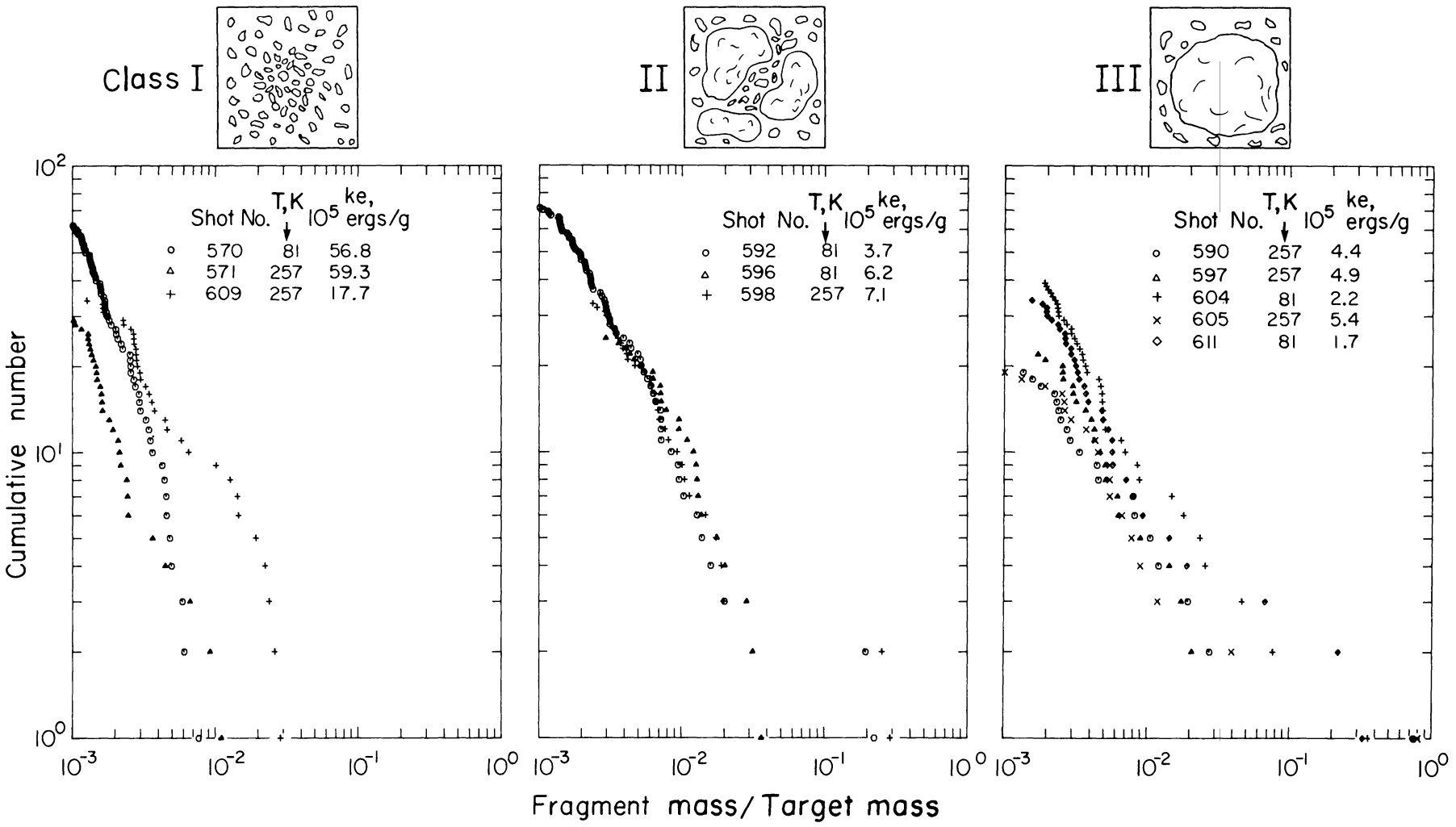


**Fig. 5.** Cumulative number of fragments vs. relative fragment weight.

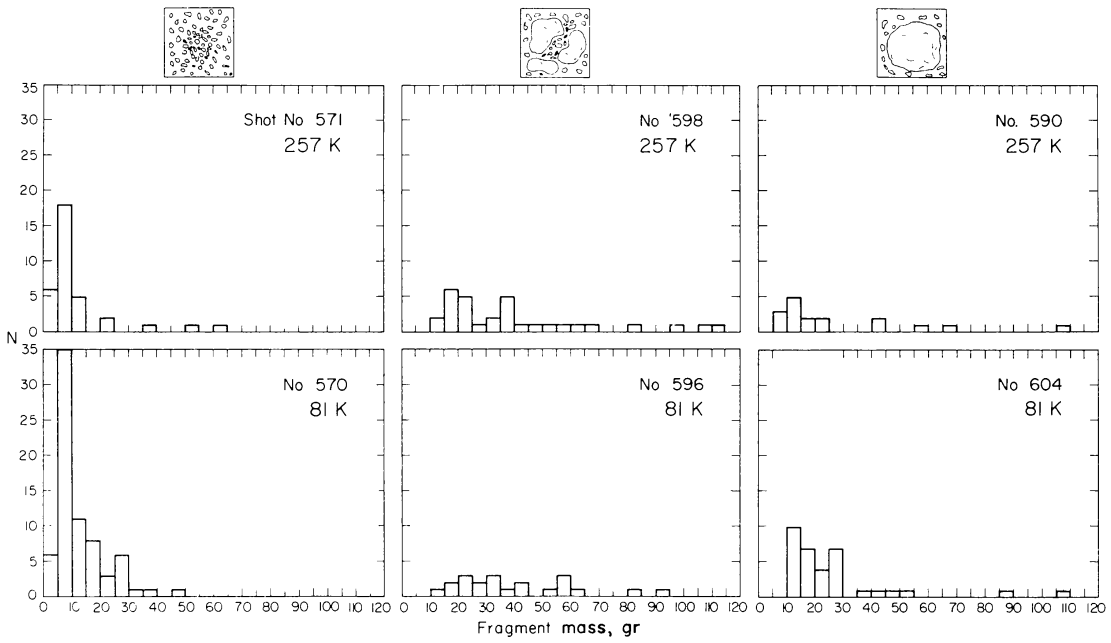


**Fig. 6.** Histograms of fragment number, N, vs. fragment mass for six class I to III experiments. Data for small fragments, with masses $<5$ g are incomplete.

In order to determine the relation between fragment mass and fragment shape in our experiments, we calculated the sphericity $\psi$ for the resulting fragments. $\psi$ is defined as

$$\psi = (V_p/V_s)^{1/3} \tag{2}$$

where $V_p$ is the volume of the fragment and $V_s$ is the volume of the smallest sphere that encloses the fragment (Friedmann and Sanders, 1978). Hörz (1969) points out that fragments originating from an experimental impact crater in granite became increasingly flattened with increasing fragment size (or fragment mass), i.e., he notes that the sphericity of his fragments decreases with increasing fragment mass. Although he defines sphericity in a slightly different way as we do, we attempted to test whether our fragments show a similar tendency. Our measurements allow the computation of $\psi$, since the fragment mass m and the mean density of ice $\rho$ at $\sim 257$ K (i.e., the temperature at which the fragments were measured; $\rho = 0.019$ g/cm$^3$; Hobbs, 1974) yield the value of $V_p$. $V_s$, a sphere with diameter A, can also be calculated for our fragments. Hence, we can rewrite equation (2) as follows:

$$\psi = 1/\mathrm{A\ K\ m}^{1/3} \tag{3}$$

where

$$\mathrm{K} = (6/\pi\rho)^{1/3} = 1.276\ \mathrm{cm\ g}^{-1/3}$$

The values of the sphericity $\psi$ as a function of fragment mass for six of our experiments are given in Fig. 11, whereas Table 3 gives the mean values of $\psi$. As can be seen, there is no clear correlation between $\psi$ and m in disagreement with the observations of Hörz (1969) on fragments from an impact crater in granite. However, as already seen in Figs. 9 and 10, the sphericity of the fragments increases with decreasing temperature (with the exception of shot 571 and 609, which represent fragmentation type I for 257 K targets). The mean values of $\psi$ are 0.73 and 0.53 for all of the 81 K and 257 K targets, respectively.

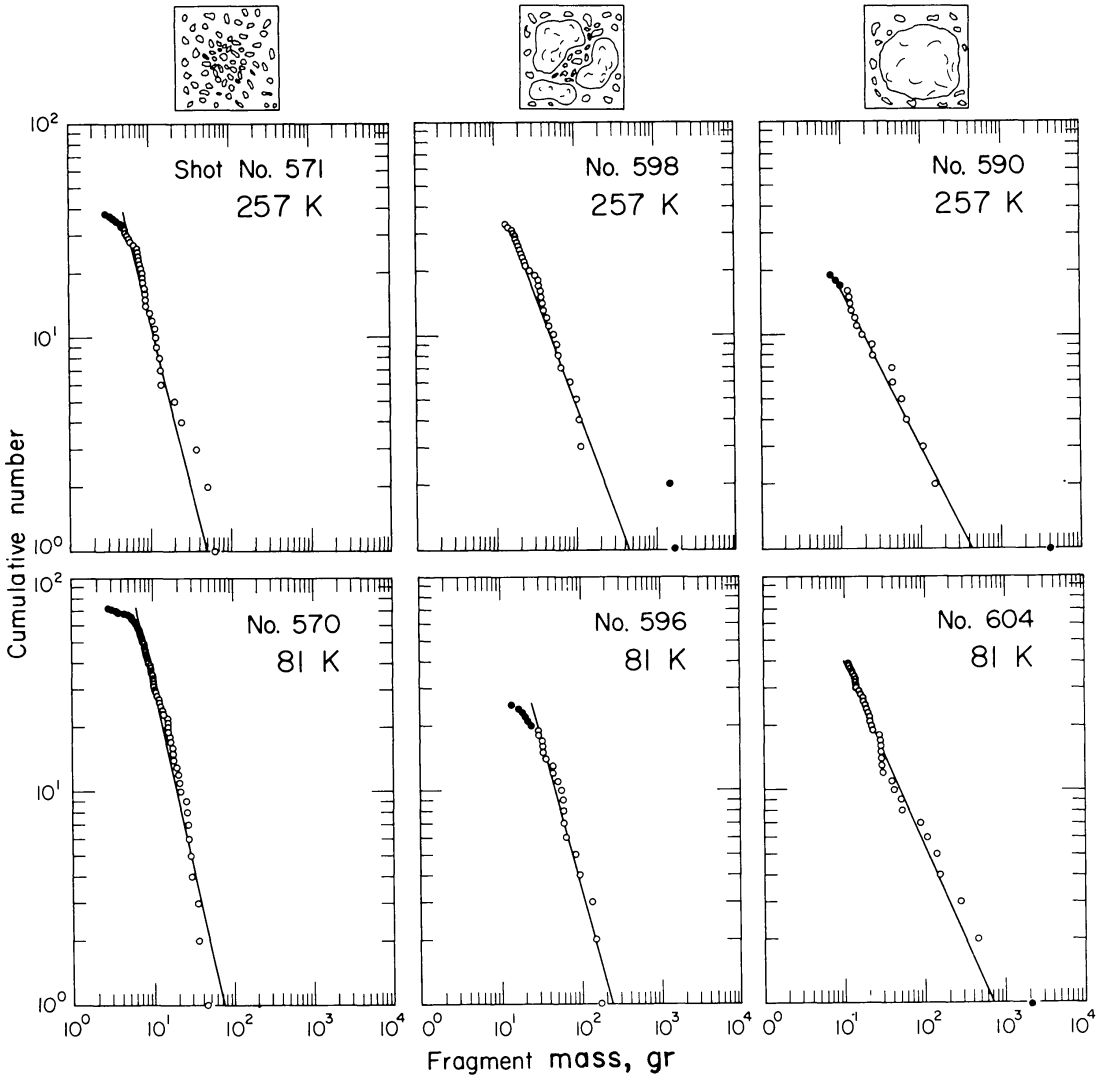


**Fig. 7.** Cumulative number of fragments vs. fragment mass for same data as in Fig. 6. Solid lines are regression fits for data represented by open symbols.

## 4. DISCUSSION AND CONCLUSION

The present experiments suggest the following conclusions. The mass ratio of the largest fragment to the target is an empirical measure representing the character of a particular impact event. It is used to assign each impact to one of the fragmentation classes as defined above, as well as to determine the transition between the fragmentation classes with respect to the required impact energies. Figure 12 gives mass ratios of largest fragment to target, $M_{lf}/M_T$, as a function of the specific kinetic energy *ke* of the projectile. The values of $ke_c$ for the transition between the fragmentation classes (also marked in Fig. 12) are given in Table 4. As can be seen, the data points clearly fall into two distinct groups, each representing a different target temperature. The threshold specific energies $ke_c$ for 257 K targets are $\sim 2$ to 3 times higher than for the 81 K targets. However, the curves for both target temperatures are nearly parallel, both covering a range of about 1.5 orders of magnitude in *ke*. Fujiwara (1980), based on the definition of destruction types by Fujiwara *et al.* (1977) gives explicit numbers for critical specific energies $ke_c$ for the transition between the destruction types (Fig. 12). These energies, together with the mean values of B/A and C/A for basalt (Fujiwara *et al.*, 1978) and data of Hartmann (1980) and Hartmann

**Table 3.** Details of experimental results for fragmentation types I–III.

| Shot No. | Fragm. Type | $T_T$, K | $C^+$ | $b^+$ | B/A* | C/A* | Sphericity* |
|---|---|---|---|---|---|---|---|
| 570 | I | 81 | 3.28 | 1.76 | 0.75 | 0.55 | 0.71 |
| 571 | I | 257 | 2.68 | 1.57 | 0.76 | 0.49 | 0.72 |
| 609 | I | 257 | 3.01 | 1.35 | 0.76 | 0.58 | 0.77 |
| 592 | II | 81 | 2.81 | 1.06 | 0.75 | 0.46 | 0.72 |
| 596 | II | 81 | 3.46 | 1.46 | 0.79 | 0.56 | 0.77 |
| 598 | II | 257 | 2.79 | 1.06 | 0.63 | 0.38 | 0.60 |
| 590 | III | 257 | 1.98 | 0.75 | 0.58 | 0.32 | 0.55 |
| 597 | III | 257 | 2.44 | 0.98 | 0.55 | 0.34 | 0.57 |
| 604 | III | 81 | 2.49 | 0.88 | 0.73 | 0.50 | 0.71 |
| 605 | III | 257 | 2.41 | 0.99 | 0.54 | 0.32 | 0.55 |
| 611 | III | 81 | 2.54 | 0.99 | 0.76 | 0.56 | 0.74 |

$^+$Coefficients for fragment weight distributions in:

$$\mathrm{Log_{10}}n = C - b\,\mathrm{Log_{10}}m$$

n = cumulative number
m = fragment mass

*Mean values

and Cruikshank (1978) are given in Table 4. As can be seen, the destruction of a silicate body requires energies about one to two orders of magnitude higher than those for an icy body. The data for water ice by Hartmann (1978) indicate critical specific energies $ke_c$ of $\sim 10^5$ ergs/g for the transition from class IV to III and $\sim 10^6$ ergs/g for the transition from III to II. Although Hartmann's data represent a different experimental approach they agree with our results for the 257 K targets (see Table 4). This indicates that the

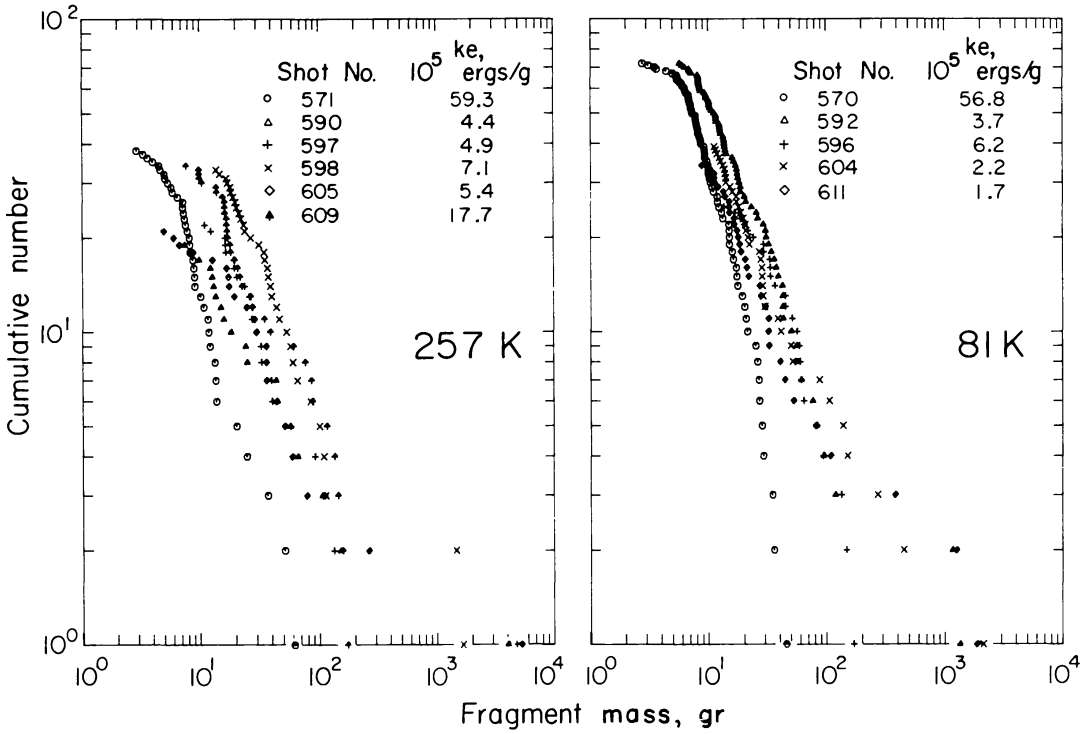


**Fig. 8.** Cumulative number of fragments vs. fragment mass for 257 K (left diagram) and 81 K (right diagram) target temperatures.

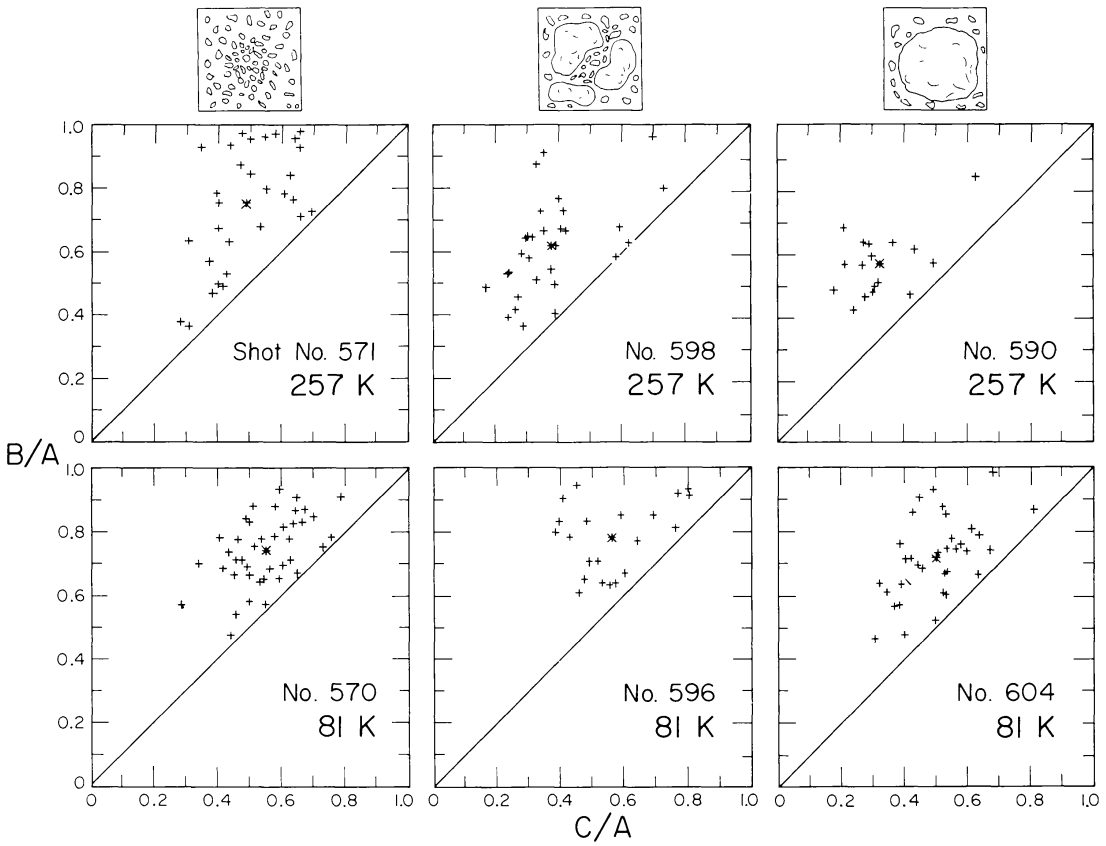


**Fig. 9.** Fragment shape factors (B/A and C/A) from class I, II, and III experiments. A is the long, B the intermediate, and C the short axis of each fragment. Mean values of B/A and C/A are shown as (*).

difference in the experimental techniques between Hartmann's and our study, as well as the difference in the combination of projectile and target materials (ice and rock vs. Lexan and ice) has only limited influence on the final results.

Fujiwara *et al.* (1977) discuss the applicability of the $ke_c$ scaling with respect to a wider range of values of the specific kinetic energy of projectiles as found in natural impacts. They suggest that the phenomena arising from the propagation of shock waves in a target body are similar, if the imparted energies per unit mass are the same. This conclusion is based, in part, on the agreement between Fujiwara *et al.*'s and Gault and Wedekind's (1969) experimental results which both give threshold energies $ke_c$ for basaltic and glass bodies, respectively, which are similar, when the difference in target strength is taken into account. While the values of $ke_c$ for basalt are about two to three times higher than those for glass (see Fig. 10 in Fujiwara *et al.*, 1977), the difference in quasi-static strength of glass ($\sim$ 1.5–2 kb; Gault and Wedekind, 1969) and typical basalt ($\sim$ 3 kb; Handin, 1966) also amounts to a factor of two. However, the differences in mass and velocity between the two groups of experiments is quite large (impact velocities of Gault and Wedekind's experiments were up to three times higher than those of Fujiwara *et al.*, whereas target masses were up to 20 times larger in Fujiwara *et al.*'s experiments). Our results support Fujiwara *et al.*'s (1977) conclusion. Impact velocities in our experiments were as much as two times lower and target masses were at least twice as large as those of Fujiwara *et al.* However, the differences in $ke_c$ between Fujiwara *et al.*'s and our experiments, as seen in Fig. 12, can be explained by the about two orders of magnitude difference in ultimate unconfined strength between basalt and water ice. Hence, the results of Gault and Wedekind (1969), Fujiwara *et al.* (1977), and the present study, which cover a range of *ke* from $10^5$ to $10^8$ ergs/g, seem to be consistent, when differences in the material properties of target materials are taken into account. Consequently, it appears that the processes

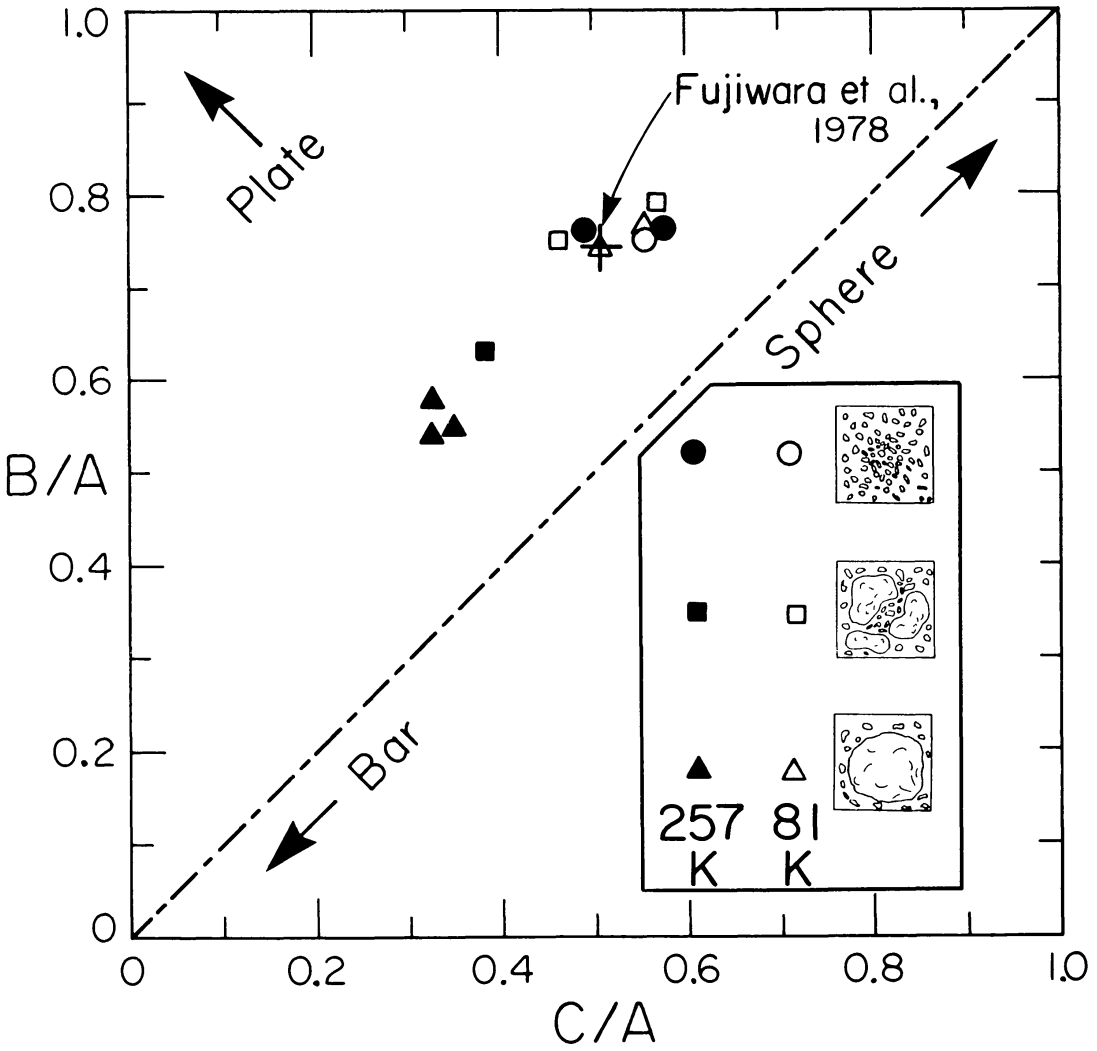


**Fig. 10.** Mean values of shape factors (B/A and C/A) from I to III fragmentation experiments. The cross at B/A = 0.73 and C/A = 0.50 is the mean value for 719 basaltic fragments given by Fujiwara *et al.* (1978).

related to impact fragmentation of a body can be described in terms of *ke* over a range of target masses of grams to kilograms and impact velocities in the 0.1 to 6 km/sec range.

The mass distribution of fragments resulting from the erosion, disruption, and total destruction of an icy body in our impact experiments can be described by a single power law relation [Eq. (1)], for fragment masses of up to $\sim 0.1$ times the target mass. The slopes b of the distributions vary between $-0.9$ and $-1.8$ and decrease with increasing specific projectile energy *ke* (or grade of fragmentation). Table 4 gives the mean values of b for our experiments with regard to fragmentation class and target temperature. It can be seen that there is no clear relation between b and target temperature. These results suggest that with increasing values of *ke* the number of small fragments in a given size range increase relative to large fragments regardless of temperature. The b values of our experiments are in good agreement with results of Fujiwara *et al.* (1977) for basalt, who find values of b of up to 1.7, and to a lesser extent with data on terrestrial and extraterrestrial rock fragments as given by Hartmann (1969) which show b values in the range from $\sim 0.6$ to 1.2. However, Hartmann (1980) also found $b = 0.96$ for an experimentally destructed artificial aggregate material.

The shapes of the fragments in our experiments have been described in terms of shape factors (i.e., ratios between intermediate and long axis and ratios between short and long axis, B/A and C/A, resp.) and the sphericity $\psi$ of each fragment. Mean values of B/A,

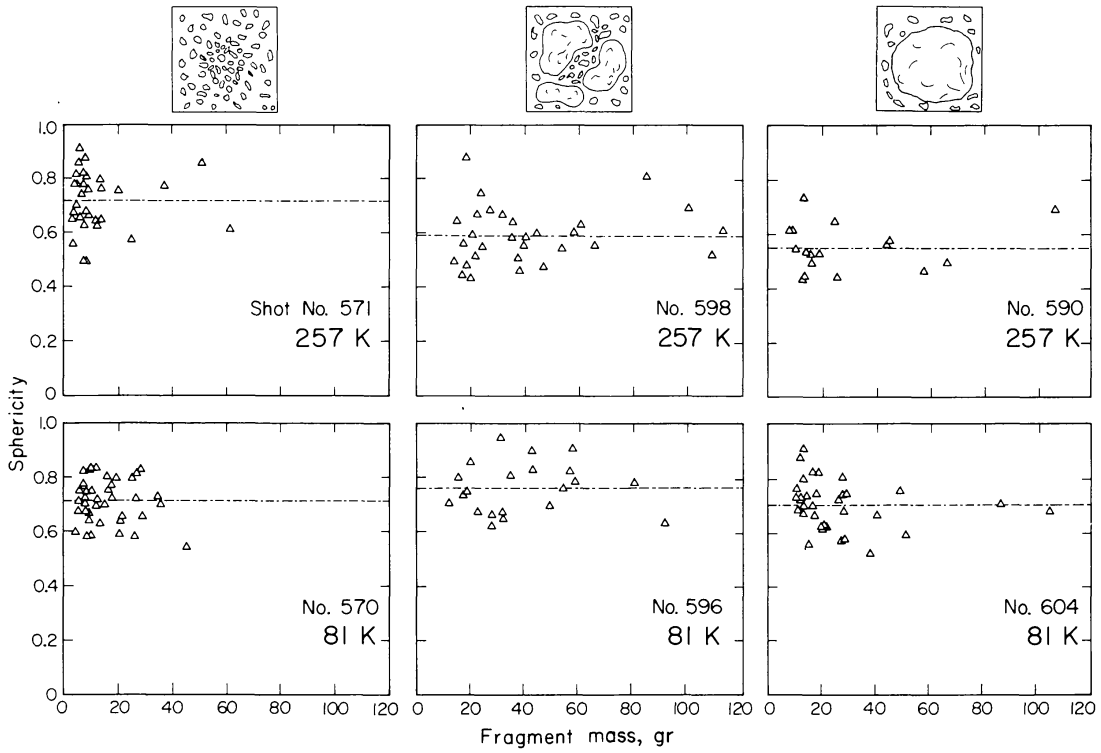


**Fig. 11.** Fragment sphericity, as defined in Eqs. (2) and (3), vs. fragment mass. The dash-dotted horizontal lines give the mean values for each experiment.

C/A, and $\psi$ with respect to fragmentation class and temperature are given in Table 4. We find that fragments from destruction of 257 K targets are less spherical than those from 81 K targets. While the former have increasing values of B/A, C/A, and $\psi$ with increasing specific projectile energy *ke*, the latter reveal no clear dependence of shape on fragmentation class. This is illustrated in Figs. 10 and 13. The straight lines in Fig. 13 represent linear regression fits to each set of data points. The slopes of the regression lines are given by $-1.5\times10^{-8}$ and $3.6\times10^{-8}$ g/ergs for the 81 and 257 K targets, respectively. The shape factors of the 81 K fragments as well as those of the 257 K targets of class I impacts agree well with values for impact fragmented basaltic targets of Fujiwara *et al.* (1978) and those for experimentally destructed igneous rocks of Hartmann and Cruikshank (1978). The fragment shapes in our experiments are found to be independent on fragment mass.

In the present experiments, we believe that most of the fragmentation occurred upon nucleation of tensile failure surfaces on crack like flaws and on air bubbles in the samples. We observed that with increasing growth rate of ice crystals, the number of air bubbles in ice increases, whereas their size decreases (Hobbs, 1974). Since the growth rate in our 81 K ice reached values of up to $\sim2\times10^{-4}$ m/s vs. $\sim10^{-5}$ m/s in the 257 K targets, the colder targets contained significantly more, but smaller voids. Hence, we believe that more tensile fractures initiated and intersected in the 81 K ice than in the warmer targets. This we propose leads to a more efficient fragmentation of 81 K targets compared to 257 K targets. Secondly, an inherent difference in both target types is the different amount of volume change suffered by the target blocks ($-1.8\%$ vs. $-0.3\%$ of the total volume for 81 K and 257 K, respectively; Hobbs, 1974). Even though, a large fraction of the contraction in the colder targets could be relieved by the technique described in section 2, it is expected that the number of initial microcracks is substantially larger than in the 257 K targets. Side spallation, or spallation of outer surface layers was relatively scarce in our experiments (with the exception of class III fragmentation in

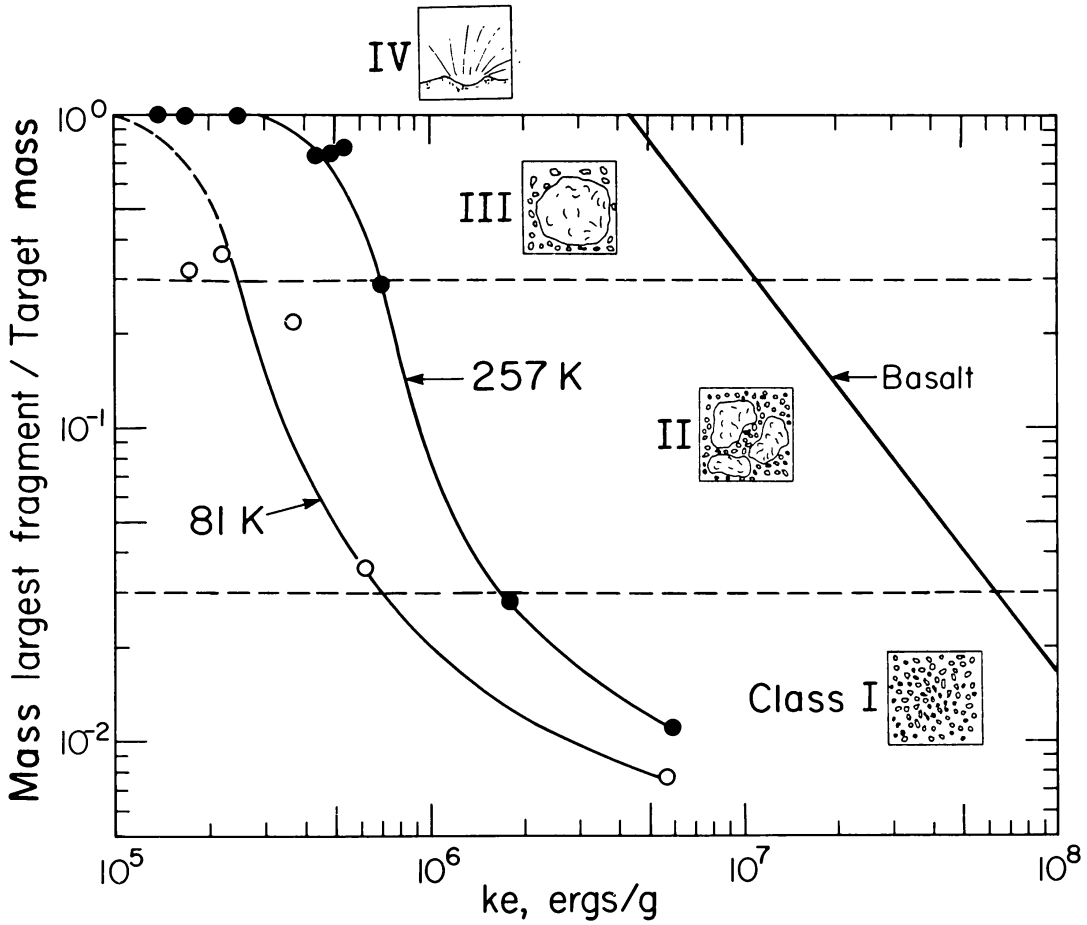


**Fig. 12.** Relative mass of largest fragment vs. specific kinetic energy of projectiles. Transition from class I to II fragmentation (at relative fragment weight of 0.03) and from class II to III fragmentation (at relative fragment weight of 0.3) is indicated.

257 K targets). This is mainly due to the relatively low peak stresses and the comparatively large target size. This leads to the absence of core type destruction, where the outer parts of the impacted body spall off, leaving a relatively undamaged core of the original body (Gault and Wedekind, 1969; Fujiwara *et al.*, 1977).

An understanding of the importance of pre-cracking, as well as of the role of air bubbles in target blocks, for the fragmentation process requires a closer look at the mechanism of fracturing. Fracturing has been studied statistically under the presumption that whenever a large number of microscopic flaws becomes activated, the failure process may be statistically averaged and may yield a usable continuum description of fragmentation (e.g., Gilvarry, 1961). Microscopic fracture theories on the other hand attempt to describe explicitly the small scale rate processes which lead to failure. Curran and his co-workers have used the latter approach to derive a quantitative analytical model of the fracturing process (Curran *et al.*, 1973; Shockey *et al.*, 1974; Curran *et al.*, 1977). At the present stage of our study, quantitative data which constrain the major processes in the Curran *et al.*, models are missing. Hence, we have qualitatively applied only the basic ideas of the first step in their models, namely the activation of preexisting structural flaws, to our problem. The two principal flaws in ice crystals grown from a fluid are homogeneously dispersed, roughly spherical, air-filled voids and randomly positioned sharper, crack like flaws (Hobbs, 1974). Both flaw types have been readily observed in all of our target blocks. Shock damage will initiate primarily at the crack like flaws, because stress will be more efficiently concentrated and flaws become unstable at lower nominal stress at these points than at the bubble like voids (Curran *et al.*, 1973).

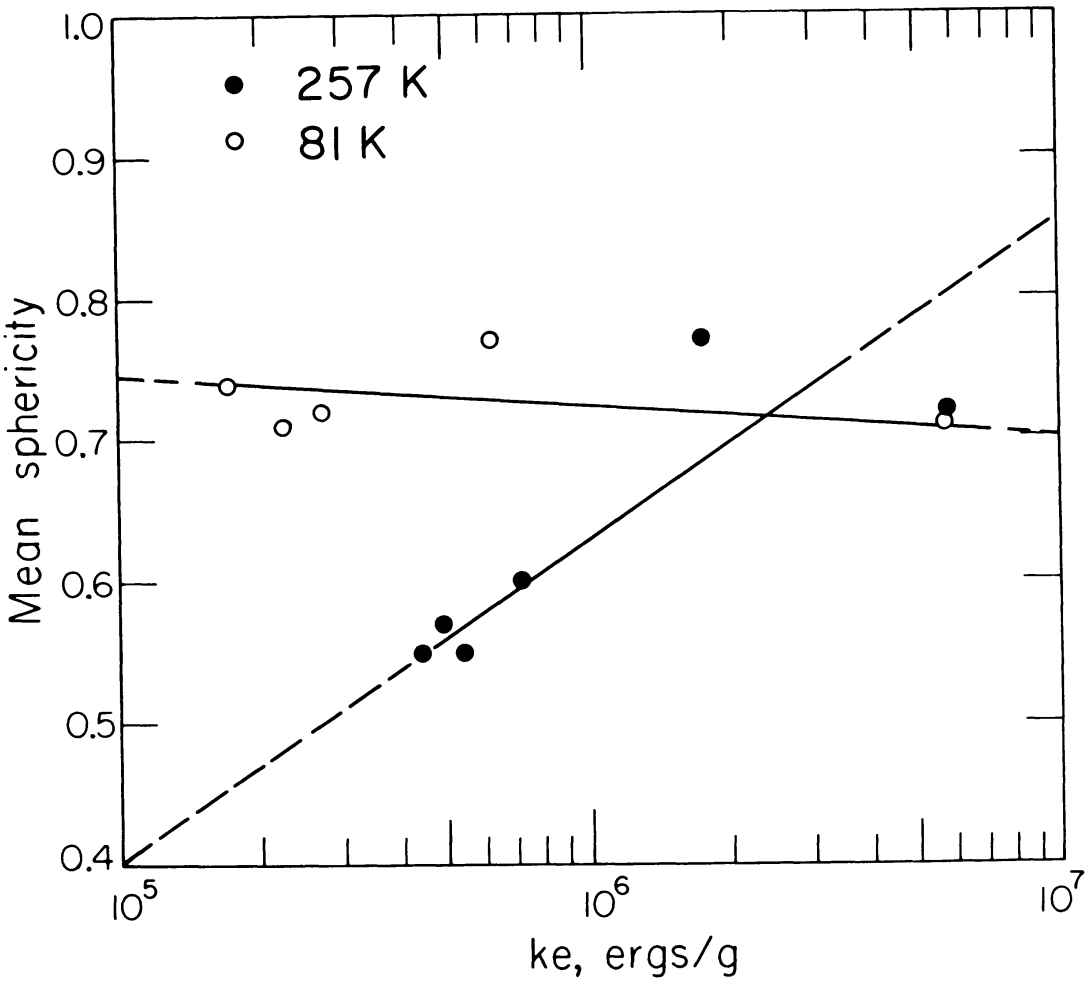


**Fig. 13.** Mean sphericity of fragments vs. specific projectile energy *ke*. Solid lines through the data represent regression lines.

**Table 4.** Summary of experimental results.

| Target Temp., K | $ke_c$ for transition from: I–II | II–III | III–IV | b* I | II | III | B/A* I | II | III | C/A* I | II | III | $\psi$* I | II | III |
|---|---|---|---|---|---|---|---|---|---|---|---|---|---|---|---|
| | | ergs/g | | | | | | | | | | | | | |
| 257 | $1.7\times10^6$ | $7.1\times10^5$ | $2.9\times10^5$ | 1.5 | 1.1 | 0.9 | 0.8 | 0.6 | 0.5 | 0.5 | 0.4 | 0.3 | 0.8 | 0.6 | 0.5 |
| 81 | $7.0\times10^5$ | $2.5\times10^5$ | $1.0\times10^5$ | 1.8 | 1.3 | 0.9 | 0.8 | 0.8 | 0.8 | 0.6 | 0.5 | 0.5 | 0.7 | 0.7 | 0.7 |
| Basalt[$] | $1.0\times10^8$ | $1.0\times10^7$ | $4.0\times10^6$ | | | | $0.7^+$ | | | $0.5^+$ | | | | | |
| Igneous rocks[#] | | | | | | | 0.7 | | | | | | | | |
| Artificial aggregate[‖] | | | | | 1.0 | | | | | | | | | | |

*Mean values.
[$]From Fujiwara, 1980.
[+]From Fujiwara *et al.*, 1978.
[#]From Hartmann and Cruikshank (1978).
[‖]From Hartmann (1980).

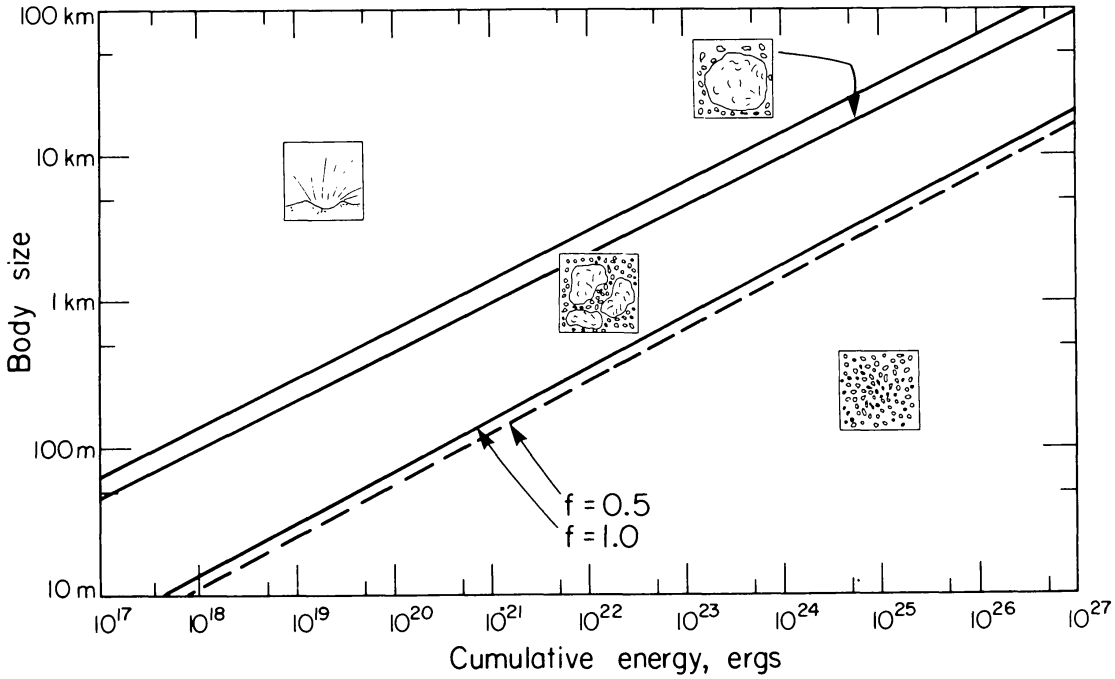


**Fig. 14.** Critical size of target body vs. cumulative energy of impactors. The solid and dashed lines mark the transition between different types of fragmentation suffered by the target, when hit by a number of impactors (or a single body) with a particular total energy. Each field between the solid lines in this diagram represents a type of fragmentation in the body size-energy plane depicted by the cartoons. f is the fraction of the total impact energy shared by the impacted body [Eq. (6)]. Differences in the results with regard to variation in f are identical for all of the three boundaries shown.

We therefore conclude that fracturing in our ice targets is initially, i.e., at low stress levels, controlled by the preexisting microcracks. However, at higher stresses, cracks will be initiated at the voids with equal efficiency. Since the bubbles are generally more numerous than the microcracks, the former will control crack initiation at higher stress levels (Curran *et al.*, 1973). As outlined above, the two target types can be distinguished in that the 81 K ice includes a larger number of microcracks as well as air bubbles (of relatively small size) as compared to the 257 K ice. We believe that both of these factors lead to more extensive fragmentation of the colder targets with respect to either the stress level necessary for crack initiation, or the number of crack nucleation sites at higher stress levels.

The differences in fragment shape as a function of target temperature (see Figs. 10 and 13 and Tables 3 and 4) can also be explained in the light of the foregoing discussions. Since activation of a larger number of flaws occurs at relatively low stresses in the 81 K ice numerous fracture surfaces and thus more regularly shaped fragments are produced as compared to 257 K ice. However, at high stress levels (i.e., in class I fragmentation), the relatively large number of air bubbles controls crack initiation and allows the formation of more numerous fracture surfaces and thus more spherical fragments for both 81 K and 257 K ice, in agreement with our results.

## 5. APPLICATIONS

Applications of our experimental results to accretion and surface evolution of icy planetary objects is restricted to the 81 K targets. Temperatures in the region of the solar nebula where abundant water ice could have been accreted correspond to a range from ~40 to ~150 K (Lewis, 1974). Present mean surface temperatures of the Galilean and Saturnian satellites, which are the prime examples for icy planetary objects in our solar

system, are $120 \pm 10$ K and $70 \pm 10$ K, respectively (e.g., Smith *et al.*, 1979, 1981). Major obstacles in applying our small scale laboratory impact experiments to natural processes on icy planets are the differences in size and shape and the differences in internal structure and bulk composition.

Fujiwara (1980) discusses the importance of the first factors with regard to his experiments on cubic basalt targets (Fujiwara *et al.*, 1977). He suggests that different shapes of experimental and planetary bodies are less restrictive as long as the aspect ratios for both groups of bodies is close to one. Based on scaling relations for cratering on gravity free bodies he also suggests that the dimensions of his targets (up to 10 cm sidelength) allow application to bodies of up to 100 km size. We adopt these considerations and infer that our results (obtained for cubic targets of $\sim 19$ cm sidelength) can be applied to accreting icy planets of $\leq \sim 100$ km radius. The size difference is less important with regard to regolith development as long as surface gravity is not a dominant parameter.

The differences in the internal structure and bulk composition of our targets and icy planets is a more severe problem. Accretion of icy planets probably involved a variety of aggregates reaching from loosly bound, highly porous "dirty snowballs" (i.e., mixtures of fine grained ice and silicates) to solid icy bodies (e.g. Hartmann, 1978). In contrast, our target blocks represent ice grown from the liquid phase thus only representing one type of icy planetesimals. Furthermore, mean densities of the icy Galilean and Saturnian satellites suggest that they contain significant fractions of silicates. This implies that accreting planetesimals consisted either of ice-silicate mixtures or that two groups of planetesimals, consisting of either ice or silicates, formed these bodies. The destruction of ice-silicate targets is a problem we have not yet addressed. Hence, the present results for pure prefractured and prestressed ice are restricted to the interaction of solid icy bodies. The crusts of the Galilean and Saturnian satellites are likely to be also multiply prefractured and prestressed. For targets of this type, Gault and Wedekind (1969) demonstrate that multiple and single impacts lead to comparable fragmentation if the cumulative energy of the multiple events equals the single impact energy. Hence, we imply in the following that energies for disruption of icy objects refer to the total energy of multiple events.

With these cautionary notes in mind, we first apply our results to the accretion of icy planetesimals. The collision of finite sized bodies requires separation of energies associated with the motion of the center-of-mass and with motions relative to it. For the latter, the impact energy, IE, is given by:

$$IE = 1/2\, M_t M_p v^2/(M_t + M_p) \quad (4)$$

(Fujiwara *et al.*, 1977)

where $M_t$ and $M_p$ are target and projectile mass, respectively, and v is the velocity of the projectile. We assume that a fraction f of this energy is shared by the target and a fraction (1–f) by the projectile (f depends e.g., on the ratio between projectile and target mass). Hence, we reformulate Eq. (4):

$$IE = M_t/(M_t + M_p) KE\, f \quad (5)$$

where KE is the projectile kinetic energy. In order to determine the limiting size, $R_c$, of an impacted body at which damage according to one of the above defined fragmentation classes occurs, we equate IE with the product of $ke_c$ and $M_t$, where $ke_c$ is the critical transition energy as defined in the previous section. This leads to:

$$ke_c = KE\, f/(M_t + M_p)$$

which yields:

$$R_c = [3/4\pi\rho_t)(KE/ke_c\, f - M_p)]^{1/3} \quad (6)$$

where $\rho_t$ is the mean density of the target body ($\sim 1$ g/cm$^3$). Insertion of $ke_c$ for our 81 K targets (see Table 4) results in critical sizes (i.e., radii) for target bodies which define regions of cratering, erosion, disruption, and total fragmentation in the $R_c$–KE plane.

Figure 14 illustrates the results of these calculations in terms of cumulative energy vs. target size for plausible limits of f. As can be seen, variation in f has only minor effects on the critical size of the impacted body. Figure 14 allows specification of the fate of an impacted icy planetesimal of certain size, when hit by impactors with *total* energy KE. It should be noted that these results are strictly valid only for low velocity impacts (i.e., v up to $\sim 1$ km/s). Values for basaltic targets, corresponding to our transition from erosion to disruption of a body, lie at $\sim 10^{18}$ to $10^{28}$ for body sizes between 50 m and 100 km (Fujiwara, 1980). We also note that for the fragmentation of an icy planet its finite gravity has to be taken into account. Hence, even though the energy of impacting bodies might be sufficient to completely fragment the planet, separation of the fragments against the gravity field of the planet requires additional energy to be provided by the impactors. Therefore, the total energies KE in Fig. 14, defining critical sizes for the destruction of icy planetesimals have to be understood as *minimum* energies.

With regard to regolith development on icy planets (we neglect in the following the effects of silicates, mixed in the crustal layers of these bodies and assume pure water ice crusts), we predict that the shapes of regolith particles in the milimeter to centimeter range are essentially spherical (or regularly formed). The mass distribution of regolith components with masses from $\sim 5$ to $\sim 160$ g, should follow a power law with a slope of $\sim -1.8$ (the slope for the cumulative size distribution equals three times the slope for the mass distribution; Hartmann, 1969). Existing observational radio- and radar reflectance data of icy regoliths are as yet not conclusive (Muhleman, pers. comm.) and cannot be used to confirm this prediction. We note however that our predicted properties of icy regoliths are comparable to those of rocky planets (Hartmann, 1969).

In the case of icy planetary rings, e.g., Saturn's ring system, more complete data are available. These data suggest mean sizes of ring particles in the centimeter to meter range and can best be fit with nearly spherical bodies (Pollack, 1975). Greenberg *et al.* (1977), based on a variety of theoretical and observational results, have attempted to predict the size distribution of particles in Saturn's rings. They find that particle sizes should follow a power law [similar to our Eq. (1)], with slopes between $-3.0$ to $-3.5$, which correspond to cumulative mass distribution indices of $-0.67$ to $-0.83$. Based on our results for 81 K ice, we predict a much steeper slope for the cumulative mass distribution, namely $\sim -1.5$. This is the mean of b values for fragmentation classes I and II (see Table 4). Greenberg *et al.* exclude a steeper mass distribution of ring particles based on the assumption that $\sim 10\%$ of the cross section of the rings resides in particles larger than 50 m in radius whereas our result (when extrapolated to this size range) imply that 50 m particles comprise $\sim 3\%$ of the total population. We assume that Saturn's rings were formed initially by the collisional destruction of a single or several large bodies, at the present location of the rings (Pollack, 1975; Greenberg *et al.*, 1977). Hence, we strictly predict only the initial size distribution of ring particles. However, the subsequent collisional interaction of bodies in the rings would tend to produce even smaller particles and thus further steepen the mass distribution.

**Acknowledgments**—The technical assistance of W. Ginn, P. Gelle and M. Long is gratefully acknowledged. We thank S. K. Croft and W. K. Hartmann for constructive and helpful reviews. This work was supported under NASA grant NSG-7129. One of the authors (M. A. Lange) received a grant from the Deutsche Forschungsgemeinschaft. Contribution No. 3611, Division of Geological and Planetary Sciences, California Institute of Technology, Pasadena, California 91125.

## REFERENCES

Anderson G. D. (1968) The equation of state of ice and composite frozen soil material. *CRREL Report* **257**, Hanover, N. H. 50 pp.

Butkovich T. R. (1954) The ultimate strength of ice. *SIRPE Res. Rep.* **15**, 12.

Croft S. K., Kieffer S. W., and Ahrens T. J. (1979) Low-velocity impact craters in ice and ice-saturated sand with implications for martian crater count ages. *J. Geophys. Res.* **84**, 8023–8032.

Curran D. R., Seaman L., and Shockey D. A. (1977) Dynamic failure in solids. *Physics Today* **30**, 46–55.
Curran D. R., Shockey D. A., and Seaman L. (1973) Dynamic fracture criteria for a polycarbonate. *J. Appl. Phys.* **44**, 4025–4038.
Dantl G. (1969) Elastic moduli of ice. In *Physics of Ice* (N. Riehl, B. Bullemer, and H. Engelhardt, eds.) p. 223–230, Plenum, N.Y.
Friedmann G. M. and Sanders J. E. (1978) *Principles of Sedimentology*. J. Wiley and Sons, N.Y. 792 pp.
Fujiwara A. (1980) On the mechanism of catastrophic destruction of minor planets by high-velocity impact. *Icarus* **41**, 356–364.
Fujiwara A., Kamimoto G., and Tsukamoto A. (1977) Destruction of basaltic bodies by high-velocity impact. *Icarus* **31**, 277–288.
Fujiwara A., Kamimoto G., and Tsukamoto A. (1978) Expected shape distribution of asteroids obtained from laboratory impact experiments. *Nature* **272**, 602–603.
Gault D. E. and Wedekind J. A. (1969) The destruction of tektites by micrometeoroid impact. *J. Geophys. Res.* **74**, 6780–6794.
Gilvarry J. J. (1961) Fracture of brittle solids. I. Distribution function for fragment size in single fracture (Theoretical). *J. Appl. Physics* **32**, 391–399.
Greenberg R., Davis D. R., Hartmann W. K., and Chapman C. R. (1977) Size distribution of particles in planetary rings. *Icarus* **30**, 769–779.
Greenberg R., Wacker J. F., Hartmann W. K., and Chapman C. R. (1978) Planetesimals to planets: Numerical simulation of collisional evolution. *Icarus* **35**, 1–26.
Handin J. (1966) Strength and ductility. In *Handbook of Physical Constants* (S. P. Clark, ed.), p. 223–290, *Mem. Geol. Soc. Amer.* **97**.
Hartmann W. K. (1969) Terrestrial, lunar, and interplanetary rock fragmentation. *Icarus* **10**, 201–213.
Hartmann W. K. (1978) Planet formation: Mechanism of early growth. *Icarus* **33**, 50–61.
Hartmann W. K. (1980) Continued low-velocity impact experiments at Ames Vertical Gun facility: Miscellaneous results (abstract). In *Lunar and Planetary Science XI*, p. 404–406. Lunar and Planetary Institute, Houston.
Hartmann W. K. and Cruikshank D. P. (1978) The nature of trojan asteroid 624 Hektor. *Icarus* **36**, 353–366.
Hörz F. (1969) Structural and mineralogical evaluation of an experimentally produced impact crater in granite. *Contrib. Mineral. Petrol.* **21**, 365–377.
Hobbs P. V. (1974) *Ice Physics*. Clarendon, Oxford. 837 pp.
Lewis J. S. (1974) The temperature gradient in the solar nebula. *Science* **186**, 440–443.
Oberbeck V. R. (1975) The role of ballistic erosion and sedimentation in lunar stratigraphy. *Rev. Geophys. Space Phys.* **13**, 337–362.
Pollack J. B. (1975) The rings of Saturn. *Space Sci. Rev.* **18**, 3–93.
Safranov V. S. (1972) Evolution of the protoplanetary cloud and formation of the earth and planets. NASA Technical translation F-677.
Shockey D. A., Curran D. R., Seaman L., Rosenberg J. T., and Petersen C. T. (1974) Fragmentation of rock under dynamic loads (abstract). *Int. J. Rock Mech. Sci. and Geomech.* **11**, 303–317.
Smith B. F., Soderblom L. A., Beebe R., Boyce J., Briggs G., Carr M., Collins S. A., Cook A. F., Danielson G. E., Davies M. E., Hunt G. E., Ingersoll A., Johnson T. V., Masursky H., McCauly J., Owen T., Sagan C., Shoemaker E. M., Strom S., Suomi V. E., and Veverka J. (1979) The galilean satellites and Jupiter: Voyager 2 imaging science results. *Science* **106**, 927–950.
Smith B. A., Soberblom L., Beebe R., Boyce J., Briggs G., Bunker A., Collins S. A., Hansen C. F., Johnson T. V., Mitchell J. L., Terrille R. J., Carr M., Cook A. F., Cuzzi J., Pollack J. B., Danielson G. E., Ingersoll A., Davies M. E., Hunt G. E., Masursky H., Shoemaker E., Morrison D., Owen T., Sagan C., Veverka J., Strom J., and Suomi V. E. (1981) Encounter with Saturn: Voyager I imaging science results. *Science* **212**, 163–191.